# Spatial-temporal dynamics of collective chemosensing

Bo Sun[a], Josephine Lembong[b], Valery Normand[c], Matthew Rogers[c], and Howard A. Stone[a,1]

[a]Department of Mechanical and Aerospace Engineering, Princeton University, Princeton, NJ 08544; [b]Department of Chemical and Biological Engineering, Princeton University, Princeton, NJ 08544; and [c]Firmenich Inc., Plainsboro, NJ 08536

Edited by David A. Weitz, Harvard University, Cambridge, MA, and approved March 20, 2012 (received for review December 27, 2011)

**Although the process of chemosensing by individual cells is intrisically stochastic, multicellular organisms exhibit highly regulated responses to external stimulations. Two key elements to understand the deterministic features of chemosensing are intercellular communications and the role of pacemaker cells. To characterize the collective behavior induced by these two factors, we study the spatial-temporal calcium dynamics of fibroblast cells in response to ATP stimulation. We find that closely packed cell colonies exhibit faster, more synchronized, and highly correlated responses compared to isolated cells. In addition, we demonstrate for chemosensing the existence of pacemaker cells and how the presence of gap junctions impact the first step of the collective response. By further comparing these results with the calcium dynamics of cells embedded in thin hydrogel films, where intercellular communication is only possible via diffusing molecules, we conclude that gap junctions are required for synchronized and highly correlated responses among cells in high density colonies. In addition, in high density cell colonies, both communication channels lead to calcium oscillations following the stimulation by external ATP. While the calcium oscillations associated with cells directly exposed to external flows were transient, the oscillations of hydrogel trapped cells can persist with a fundamental frequency and higher harmonics. Our observations and measurements highlight the crucial role of intercellular signaling for generating regulated spatial and temporal dynamics in cell colonies and tissues.**

emergent behavior | cell signaling

Cells constantly sense their local chemical environment and make decisions based upon the information received. This process, known as chemosensing, is intrinsically stochastic. Not only do the chemical perturbations fluctuate in space and time, but even for uniform stimulations, the responses vary significantly from cell to cell (1). Despite this variability, multicellular organisms are capable of performing highly regulated, consistent responses, which are crucial to maintain the normal functionality of complex life systems (2).

Achieving coordinated collective responses requires individual cells to exchange information with each other within the population. For example, in the process of quorum-sensing, bacteria synthesize and secrete signaling molecules into the extracellular space. Once the concentration of the molecules, which encodes information of cell density, reaches a threshold value, bacteria transform to a different state thus generating collective behavior (3). Similarly, when a population of the social amoebae *Dictyostelium discoideum* is stimulated by external cAMP (cyclic adenosine 3,5-monophosphate), more cAMP is released by each cell into the extracellular space. Because Dictyostelium undergoes quiescent to oscillatory transitions as a function of external cAMP concentration, the collective response of Dictyostelium to cAMP can be dramatically different from the response of isolated cells (4).

On the other hand, the basis of collective behavior of mammalian cells during chemosensing is much less understood, largely because mammalian cells have developed highly diversified, coupled signaling pathways that are still topics of extensive research (5). In fact, recent studies have begun to elucidate new features of mammalian cell collective chemosensing, which are uncommon for prokaryotic systems. For example, when exposed to tumour-necrosis factor, fibroblast cells yield both digital and analog outputs, while a subpopulation demonstrates much higher sensitivity compared to the average (6). The mammalian olfaction system provides another example of collective chemosensing. Using animal models, it has been shown that the temporal order within the colony of olfaction neuron cells is directly related to how information is perceived and processed by the brain (7).

In this paper, we use microfluidic devices to study group responses of mouse fibroblast cells to external ATP (adenosine triphosphate) stimulation as a model to explore the role of intercellular signaling and those cells that responded first (pacemaker cells) in regulating the collective behavior during chemosensing. Our model system involves the detection of ATP, which is an important and common signaling molecule that regulates platelet aggregation (8), vascular tone, cardiac function (9), neurotransmission, and muscle contraction (10). The cells detect ATP using P2 receptors, which are among the most abundantly expressed receptors in mammalian tissues (11). In particular, when ATP molecules bind to P2Y purinergic receptors on the cell membrane, second messengers IP3 (inositol 1,4,5 triphosphate) are released into the cytoplasm and participate in opening ion channels to release calcium ions stored in the endoplasmic reticulum (12–14). The resulting elevation of calcium concentration inside the cell can be detected in real time with various fluorescent calcium indicators, which we use to study the responses on a single cell level.

Once excited, cells are also able to exchange information through gap junctions formed between cells in physical contact, or via other released signaling molecules, which diffuse in the extracellular space (15). As we will show, while the gap junctions play a major role when the cells are exposed directly to external flow, diffusing molecules are the only means of communication when separated cells are encapsulated in hydrogel. Recognizing these two general modes of communication allows us to alter the relative importance of the two communication channels and examine how cell-cell interactions in a colony generate various emergent features during chemosensing.

## Results and Discussion

In order to study the response of fibroblast cells to ATP stimulation, we designed a microfluidic flow chamber cultured with a stepwise density of cells (Fig. 1*A*). In particular, loading the cells first using the exit, then the inlet, we covered the collagen-coated bottom of the chamber with two cell colonies with different densities adjacent to each other (see *Materials and Methods*). Extracellular ATP was delivered by flowing the ATP solution at a constant flow rate of 90 μL/min from the low cell density side to the high cell density side using a syringe pump. This flow rate

Author contributions: B.S., J.L., V.N., M.R., and H.A.S. designed research; B.S., J.L., and H.A.S. performed research; B.S., J.L., and H.A.S. analyzed data; and B.S., J.L., and H.A.S. wrote the paper.

The authors declare no conflict of interest.

This article is a PNAS Direct Submission.

See Commentary on page 7591.

[1]To whom correspondence should be addressed. E-mail: hastone@princeton.edu.

This article contains supporting information online at www.pnas.org/lookup/suppl/doi:10.1073/pnas.1121338109/-/DCSupplemental.

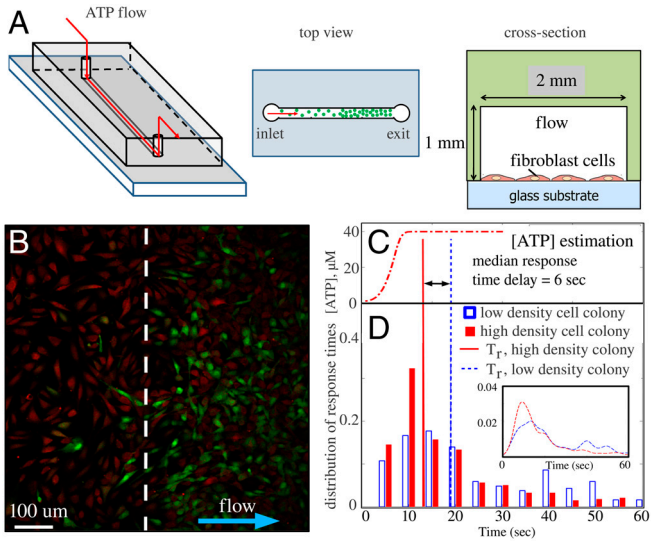


**Fig. 1.** Excitation of fibroblast cells of nonuniform spatial density by ATP. (*A*) Schematics of the flow device. (*B*) An image from the calcium imaging fluorescent video during flow of ATP solution from the low cell density colony to the high cell density colony (separated by a dashed line). Red: reference fluorescence showing cell locations. Green: fluorescent signal from calcium indicator above the reference level. (*C*) Temporal profile of ATP concentration estimated from fluorescent dye in the same flow conditions. (*D*) Histogram and probability distribution of individual cell response times for the two colonies of different densities (380 cells in the high density colony and 121 cells in the low density colony were sampled). The median response time $T_r$ is 19 sec for the low density group and 13 sec for the high density group.

ensures fast delivery across the field of view (average flow speed 750 μm/sec) without generating detectable shear-stress induced calcium responses (16). For all of our experiments we used physiologically relevant ATP concentrations, typically 10–100 μM.

To monitor the calcium response of each cell, cells were loaded with Fluo-4 calcium indicator (Invitrogen) and the fluorescent images were taken on a confocal microscope (Leica SP5) at a frame rate of 1 frame/sec with a 20x oil immersion objective. The reference fluorescent intensity $I_r$ was determined by averaging the intensities $I(t)$ during the flow of pure solvent before ATP arrived (e.g., Fig. 1*B*). For chemosensing experiments, we define the relative fluorescent intensity (RFI) $R(t) = \frac{I(t)-I_r}{I_r}$. To construct the response curve of individual cells, $R(t)$ is further averaged over 40 pixels at the center of each cell to obtain $R_i(t)$ of the cell with index $i$. After measuring the calcium response, we flushed the device with fluorescein solution under identical flow conditions. The fluorescent intensity of the fluorescein solution recorded above the cell monolayer is then used as an estimate of the temporal profile of ATP concentration and is correlated with the calcium response (Fig. 1*C*).

Our set up allows us to measure calcium dynamics of cell colonies with well controlled spatial density as well as stimulation doses. For example, in Fig. 1 *B* and *D*, we report the results of a typical experiment (Movie S1). Although 40 μM ATP was delivered to the low density cell colony first, the typical response time of cells in the high density group was faster. This result has been confirmed by multiple independent experiments and we have obtained similar results for three different solvents: HBSS (Invitrogen), HBSS without calcium and magnesium (Invitrogen), DMEM (ATCC), as well as a wide range of ATP concentrations from 20 μM to 200 μM. To evaluate the delay in response times, we define the activation time of an individual cell as it obtained a threshold intensity (Fig. S1). In Fig. 1*D*, we plot the normalized histograms of these activation times. Indeed, the median response time $T_r$ of the high density colony is 6 s faster than the low density colony (see also Fig. S2 and Movies S2 and S3).

Because the cells all came from the same source and were cultured in the same conditions, we might expect the response of cells to be a Poisson process and the distributions of activation times to be statistically identical in spite of the different cell densities. On the contrary, Fig. 1 shows that the cells in the high density group typically responded faster than the low density group. This density-dependent result is only possible if the response events were internally correlated, which we will quantify next. We note that calcium waves propagating in the opposite direction of delivered stimuli have been observed in vivo for hepatocytes (17) and was attributed to more receptors expressed in the pericentral region. Here we demonstrate an intrinsic directionality can originate purely from density-dependent cellular correlations, rather than the difference in the sensitivity of individual cells.

The above observations suggest correlations between the cellular responses, which can be evaluated using the normalized pair cross-correlation function, $C(\tau)_{ij}$, defined as

$$\dot{R}_i(t) = \frac{dR_i}{dt}(t) - \left\langle \frac{dR_i}{dt}(t) \right\rangle$$
$$C(\tau)_{ij} = \frac{1}{\sqrt{\sigma_i \sigma_j}} \left\langle \dot{R}_i(t)\dot{R}_j(t+\tau) \right\rangle. \quad [1]$$

To evaluate $\frac{dR_i}{dt}$, we numerically differentiated the response curve $R_i(t)$ using the five-point stencil method; $\langle \frac{dR_i}{dt} \rangle$ is the time average. Also, $\sigma_i$ is the variance of $\dot{R}_i(t)$, which normalizes $C(\tau)_{ij}$ to be dimensionless. Because the two main channels of cellular communication—gap junctions and extracellular diffusing messenger molecules—are both short-range interactions among nearby cells, we only consider the cross-correlation between nearest-neighbor pairs. Hence, the averaged cross-correlation function $\bar{C}(\tau)$ is obtained by averaging $C(\tau)_{ij}$ over all the nearest-neighbor pairs $i$, $j$.

First, we studied the influence of cell density on the correlations of calcium dynamics recorded for individual cells with their nearest neighbors (Fig. 2*A*). 100 μM ATP in DMEM was introduced to cell colonies of three different areal densities (Fig. 2*A*, *Inset*). At this relatively high concentration of ATP, the calcium levels of most cells were dominated by a single transient rise following the stimulation (Fig. S1) (18). However, even though the cells were exposed to ATP at the same time, the activation time varied from cell to cell and the level of synchronization among the cells is represented by the width and magnitude of the central peak in the averaged cross-correlation function. As is clear from Fig. 2*A*, closely packed cell colonies (approximately 1,000 cells/mm$^2$) displayed highly synchronized responses, while moderately distributed cells (approximately 600 cells/mm$^2$) were correlated more weakly, and sparsely distributed cells (approximately 200 cells/mm$^2$) exhibited essentially no correlations. These results are qualitatively consistent with Fig. 1*D*.

Next we investigated the influence of ATP concentrations (Fig. 2*B*). At lower concentrations of ATP (less than 50 μM), calcium dynamics of individual cells start to deviate from each other (19) and it is easier to distinguish the effect of cellular communications from the dominate role of external ATP, because the latter typically led to a single transient elevation followed by slow relaxation for most of the cells at high ATP concentrations (Fig. S1). Indeed, the weak negative correlations for 100 μM ATP as shown in Fig. 2*A* are more evident at lower ATP concentrations (Fig. 2*B*). Also the time delays of the peak negative correlations increase as the external ATP concentration increases (Fig. 2*B*, *Insets*, and Figs. S3–S5 and Movies S4–S19).

We hypothesize that the negative correlations were caused by locally transmitted second messengers between adjacent cells. After the initial stimulation by ATP, the cells slowly relaxed to

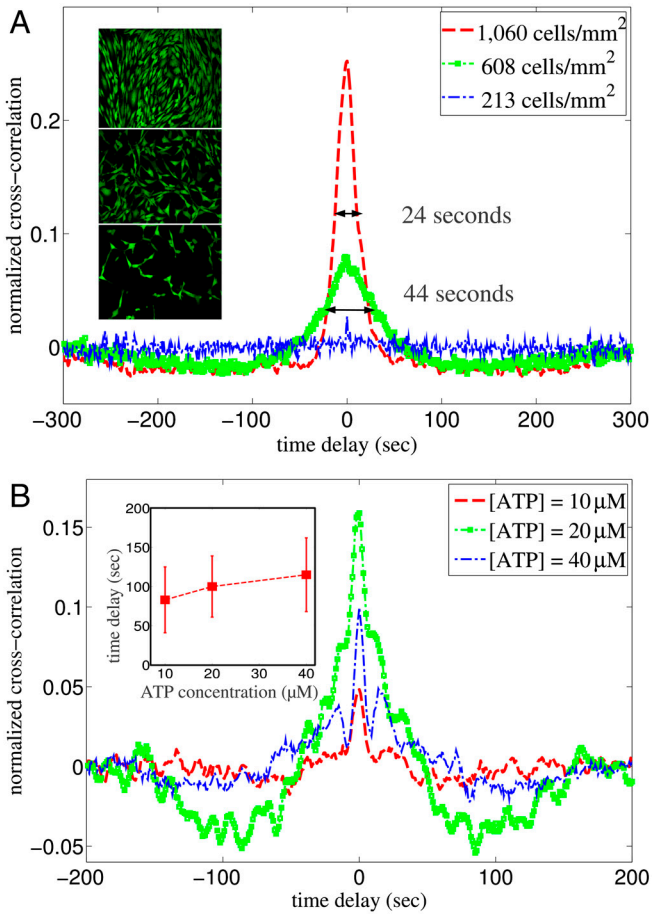


**Fig. 2.** Averaged cross-correlations of nearest neighbors as a function of cell density and ATP concentration. (*A*) Normalized cross-correlation function $\bar{C}(\tau)$ of nearest neighbors for cell colonies with different densities stimulated by 100 μM ATP in DMEM. The width of the central peak is 24 sec for the high density colony (1,060 cells/mm$^2$) and 44 sec for the medium density colony (608 cells/mm$^2$). At even lower density, the averaged cross-correlation function is almost featureless. Inset: representative images from the three experiments with different cell densities. (*B*) For densely packed cell colonies (approximately 1,000 cells/mm$^2$), reducing the stimulating ATP concentration reveals clear negative correlations between nearest neighbors. Inset: the time delays of the peak negative correlation for different ATP concentrations. Each data point represents the mean value and standard deviation calculated from 4,000 cell pairs of four independent experiments (Movies S4–S15).

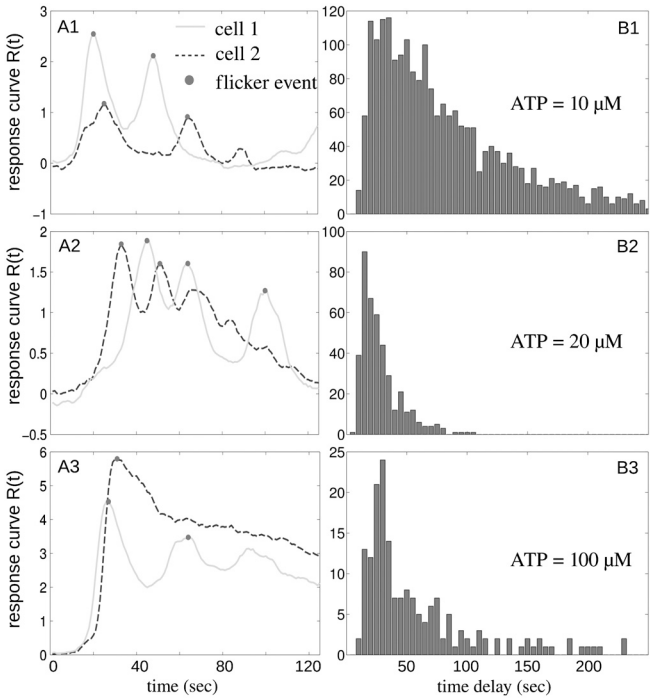


**Fig. 3.** Statistics of flicker events in a closely packed cell colony (approximately 1,000 cells/mm$^2$). (*A1*) Typical response curves of two cells (dashed and solid lines) in a densely packed colony stimulated with 10 μM ATP. The filled circles represent the flicker events defined as local maxima in the response curve. The response curve plotted covers 125 sec from the time the first cell in the colony started to respond. (*B1*) The histogram of time delays between consecutive flicker events in the same experiment as *A1*. (*A2–B2*) Similar to *A1–B1*, except the concentration of ATP is 20 μM. (*A3–B3*) Similar to *A1–B1*, except the concentration of ATP is 100 μM.

the reference state (≈1 min), after which they can be excited again by the IP3 and calcium from nearby cells. The relaxation and the second excitation produced negative correlations between the nearest-neighbor cells. The longer time delay at higher concentrations of ATP (Fig. 2*B*, *Inset*) is qualitatively consistent with the down regulation of gap junction conductance by cytoplasmic calcium ions (20).

While the calcium dynamics at high concentration of ATP (higher than 100 μM) were dominated by a single rise followed by rapid relaxation, within a closely packed cell colony we observed significant flickering in the responses at low ATP concentrations (approximately 20 μM), which demonstrated transient calcium oscillations. Representative response curves $R_i(t)$, as defined above, are plotted in Fig. 3 *A1–A3*. The flicker events were detected by locating the local maxima in the response curves. To quantify the temporal order in the calcium oscillation, we plot the histograms of the time delay between the flicker events in Fig. 3 *B1–B3*. At high concentration of ATP (100 μM), only a few flicker events were observed (Fig. 3*B3*). At very low concentration of ATP (10 μM), the event counts increased dramatically (2,200 times for 540 cells over 10 min), and the time delays demonstrated a broader distribution centered around 30 s (Fig. 3*B1*). A small increase in ATP concentration (20 μM), however, led to a much narrower distribution of time delays, while the event count was reduced because the oscillations persisted for a shorter period of time (Fig. 3*B2*).

Over the range of ATP concentrations examined, the peak oscillation frequencies stayed almost the same. Also the statistical characteristics are very different from spontaneous calcium oscillations, which are rare and much more broadly distributed (21) (see also Fig. S6). Furthermore, in low density cell colonies (approximately 200 cells/mm$^2$), few calcium oscillations were observed for ATP concentration from 10–100 μM and the time delays did not show clear statistical features. Thus, we have demonstrated that when extensive cellular communications are present, as is possible at high cell densities, extracellular ATP can induce transient calcium oscillations with a frequency of about 0.04 Hz, which is insensitive to the external ATP concentration. However, the statistics of the flicker events depend on ATP concentration, which we interpret as a result of the interplay between adaptation and cellular communications.

The collective chemosensing of cell colonies are not only characterized by the cell–cell interactions, as we have discussed, but are also influenced by the intrinsic differences from cell to cell in the population (17). For instance, some cells express more receptors than the others, thus becoming pacemakers that respond faster to external stimulation (19). To study the influence of such pacemaker cells on the response of the population, we delivered two-step pulses of ATP separated by 20 min to a densely packed colony and focused on the initial state of the response (Fig. 4 *A1–A3* and Movies S20–S21). Comparing the relative

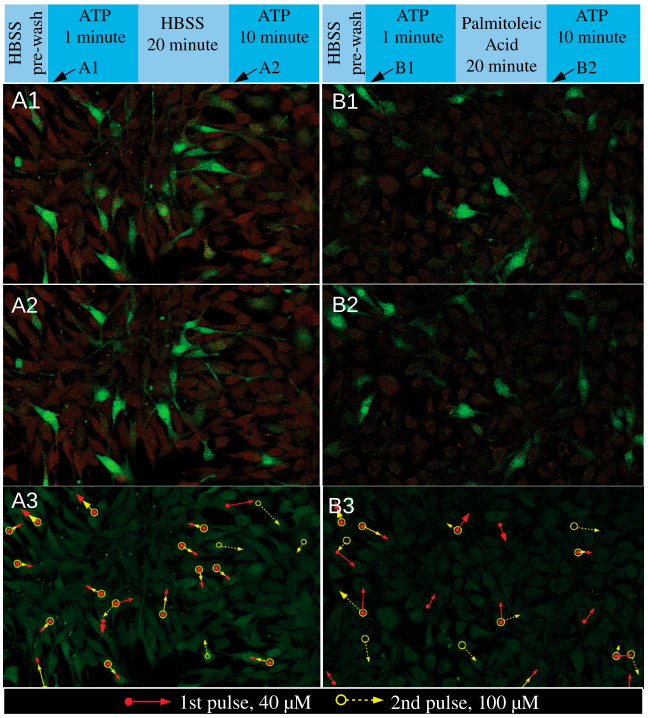


**Fig. 4.** The role of pacemaker cells and gap junctions in the early state of group response. (*A1–A3*) The response of pacemakers in a densely packed cell colony. (*A1*) Red: baseline fluorescence of calcium imaging showing the location of cells. Green: fluorescent intensity beyond the baseline. The image was taken 5 sec after the first cell responded to a 40 μM ATP pulse, while the pulse of ATP lasted 1 min and was followed by HBSS to allow the cells to relax. (*A2*) Baseline and fluorescent intensity of the same colony as in *A1*. Image was taken 6 sec after the first cell responded to a 100 μM ATP pulse and the pulse lasted 10 min (Fig. S6). In between the ATP pulses of *A1* and *A2*, cells were allowed to relax for 20 min within continuous flow of HBSS. (*A3*) Circle symbols label the cells that responded the fastest (pacemakers) in the two ATP pulses and the arrows point to the nearest-neighbor cells of the pacemakers that responded subsequently. Open circles: pacemakers of the second ATP pulse. Filled circles: pacemakers of the first ATP pulse. When the arrows overlap, only one is visible. Notice *A1–A2* covers only the upper part of *A3*. *B1–B3* is similar to *A1–A3*, except the cells were treated with palmitoleic acid for 20 min in between the two ATP pulses. Top insets: the temporal profile of the solution content delivered to the cell.

fluorescent increase in Fig. 4 *A1* and *A2*, it is clear that those cells that responded first were the same for the two separate pulses. Furthermore, we labeled these pacemaker cells in Fig. 4*A3* and use arrows pointing to their nearest neighbors that responded subsequently in the second pulse. Surprisingly, not only the pacemakers but also the temporal sequences associated with the pulse responses were preserved. Also, because the arrows appear to be oriented randomly, there is no direct correlation to the direction of the flow.

We hypothesize that this deterministic feature is a result of cellular communications, because otherwise the responses following the pacemaker cells would be random. In addition, if the cells were communicating only through extracellular diffusing molecules, all nearest neighbors would be equally exposed to the signaling molecules thus the temporal sequences would not be expected to be repeatable in the second pulse. Hence we conclude that the cells were communicating through gap junctions, which is consistent with the observations in Fig. 2.

To further examine the role of gap junctions, we performed similar experiments to the above, but treat the cells with palmitoleic acid for 20 min between the two ATP pulses. Palmitoleic acid is well accepted as a gap junction inhibitor without significantly affecting calcium response (21, 22). We hypothesize that the inhibitor should destroy the temporal order established through gap junction communication. This result was indeed what we observed, as shown in Fig. 4 *B1–B3* (also Movies S22–S23): The cells responding first in the two ATP pulses were almost the same, while the subsequent temporal orders deviated significantly (Fig. 4*B3*).

While the above experiments demonstrated the importance of gap junctions, it is intriguing to ask what type of collective behavior can result from cellular communications through diffusing molecules. To address this question, we encapsulated fibroblast cells in a thin hydrogel film (approximately 200 μm in thickness) and maintained the flow on top (Fig. 5 *A* and *B*). The cells were well separated from each other, thus we expect few gap junctions to be formed. In addition, the hydrogel protected the cells from external flows while allowing stimulating ATP molecules to reach the cell by diffusion. Because ATP can diffuse in the hydrogel approximately as fast as in water, and most cells sedimented near the bottom of the gel during the gelation process (Fig. 5*A*), it is reasonable to assume that inside the field of view, all of the cells were exposed to ATP at the same time.

To examine the density dependence of the collective chemosensing, we again created cell colonies with stepwise areal densities (Fig. 5*A*, two colonies are separated by the dashed line). Then, we studied the calcium dynamics of gel-encapsulated fibroblast cells stimulated by 100 μM ATP solution flow on top of the gel. In contrast to the observation of Fig. 1, there is no difference of the response times for the two colonies (Fig. 5*A*, Insets, and Movie S24). In fact, the activation times were broadly distributed in both colonies, which is evident from the averaged nearest-neighbor cross-correlation functions (Fig. 5*C*). As a further feature of spatial-temporal effects, we observed ATP-induced calcium oscillations in high density cell colonies (>1,500 cells/mm$^2$) embedded in hydrogel. In fact the oscillations persisted

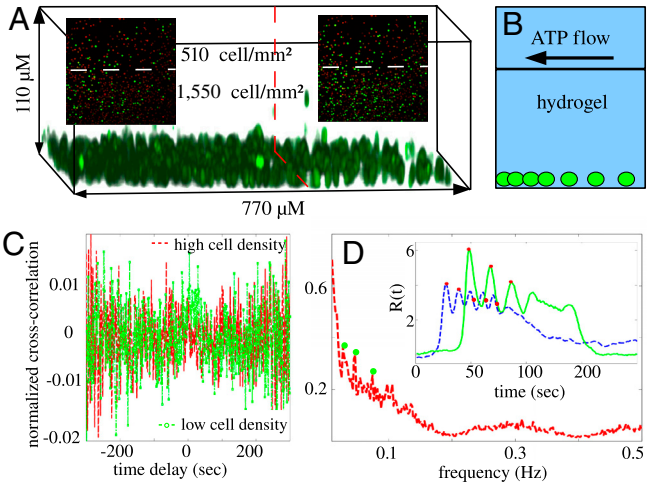


**Fig. 5.** Characteristics of the collective responses when cells were encapsulated in hydrogel. (*A*) Confocal reconstruction of fibroblast cells embbeded in hydrogel. Due to sedimentation during the gelation process, most cells were near the bottom of the gel. Cell density was constructed stepwise (boundary indicated by the dashed line) and the external ATP flow was from the low density side to the high density side. Inset: snapshot of fluorescent images showing the calcium level beyond the baseline. No distinction of response time was observed for the two colonies. Left and right insets were taken 10 sec and 30 sec, respectively, after the cells started to respond to 100 μM ATP. (*B*) Schematics of the vertical structure of the device. (*C*) Averaged cross-correlation functions between nearest neighbors in the low density cell colony and high density cell colony as shown in *A1*. (*D*) Fourier spectrum of response curve averaged over the cells in the high density colony. Filled circles locate the peaks in the spectrum. Inset: Representative response curves of two cells in the high density colony. The curves cover 200 sec from the first cell in the colony started to respond.

for a long time (approximately 10 minutes), which made it possible to study the frequency directly using Fourier analysis. We plot in Fig. 5*D* the mean spectrum obtained from averaging the fast Fourier transform of the response curves within the high density colony of Fig. 5*A*. The mean spectrum features oscillation frequencies around 0.02 Hz, 0.04 Hz and 0.06 Hz. While the frequency at 0.04 Hz also shows up in Fig. 3, further study is needed to understand the underlying mechanism that gives rise to these time scales. On the other hand, calcium oscillations in the low density colony were less significant and the frequencies differed from cell to cell making the averaged spectrum very weakly featured (Fig. S7). The comparison thus suggests a mechanism of phase-locking through intercellular signaling, whose strength increases monotonically with cell density, due to the dissipative nature of the diffusion process.

## Conclusion

We have described a systematic study of the spatial-temporal calcium dynamics of fibroblast cells collectively responding to external ATP. When the cells were directly exposed to flow of agonist, cellular communications were dominated by gap junctions. Closely packed cell colonies demonstrated rapid, synchronized, and correlated responses. Within these colonies, there were a few cells more sensitive than the others and these pacemakers led the response. Despite the stochastic nature of the process, the orders in which neighboring cells of the pacemakers responded subsequently were deterministic. This temporal order, however, was disrupted by chemically blocking gap junctions. In addition, because intercellular communications via gap junctions synchronized the responses between nearby cells, we conclude that pacemaker cells were capable of advancing the average activation times within a colony.

When the cells were encapsulated in hydrogel, cellular communications were dominated by diffusing signaling molecules. In contrast to the previous configuration, changing cell density did not significantly alter the average response time nor the level of synchronization, which further proved the role of gap junctions in the early state of collective chemosensing.

Also, we have documented ATP-induced transient calcium oscillations of individual cells in a densely packed colony, and the concentration dependence of the distribution of time delays between consecutive calcium spikes. For the case of gel-encapsulated cells, the calcium oscillation persisted much longer and the Fourier spectrum exhibits a fundamental frequency at 0.02 Hz and higher harmonics. Although extensive theoretical work on the mechanisms of intracellular calcium oscillations has been done before (23), the dependence on cellular communications is still not well understood. Our observations and measurements highlight the crucial role of intercellular signaling for generating regulated spatial and temporal dynamics in cell colonies and tissues. As a particular example, fibroblast cells sense ATP during wound healing (24) and inflammation responses 25), so that our results suggest an important role of intercellular signaling in tissue generation and remodeling.

## Materials and Methods

**Fabrication of Flow Device.** The flow device consisted of a PDMS cover on top of a collagen-coated glass slide, which creates a chamber in between for cells to adhere and different solvents to flow (Fig. 1*A*). To make PDMS covers, prepolymer of poly(dimethylsiloxane) (PDMS; Sylgard 184, Dow Corning) was poured over a stainless steel template (Wet Jet Precision), placed on a vacuum chamber to remove air bubbles, cured at 65 Celsius overnight, and peeled off the template. Surfaces of coated glass slide and PDMS cover were oxidized in plasma for 30 s to form an irreversible seal when the two surfaces were brought into contact.

**Cell Culture and Sample Preparation.** NIH 3T3 mouse fibroblast cells were cultured in Dulbecco's modified Eagle medium (DMEM; ATCC) containing 1% penicillin and 10% calf bovine serum and cultured at 37 Celsius incubator with 5% $CO_2$. To create a cell colony with stepwise density, a high density cell suspension was loaded from the outlet to fill half of the channel. After 2 to 3 h, the channel was washed gently to remove the cells that were not yet adhering to the bottom surface. Then the low density cell suspension was loaded into the whole channel. After 30–40 h of incubation, Fluo-4 calcium dye (Invitrogen) was loaded into the device. Following another 1 h of incubation, the sample was ready for imaging.

**Fluorescence Imaging and Image Analysis.** Fluorescence was detected using a confocal microscope (Leica SP5) with Argon laser at 488 nm wavelength. Movies were taken at a frame rate of 1 frame/sec with a 20x oil immersion objective. Image analysis and data process were performed in MATLAB. (Details in *SI Text*.)

**Cell Encapsulation in Hydrogel.** NIH 3T3 mouse fibroblast cells were encapsulated in biocompatible hydrogels (Extracel Hydrogel Kit, Advanced Biomatrix), which consists of glycosil (thiol-modified hyaluronan), gelin (thiol-modified gelatin), and a thiol-reactive cross-linker, polyethylene glycol diacrylate (PEGDA). Trypsinized cells were suspended in fresh growth medium and a mixture of gelin, glycosil, cross-linker, and cell suspension in following ratio: 3:3:1.5:1 was made. Two droplets (10 μL) of hydrogel solution with different cell densities were placed adjacent to each other in order to create stepwise cell density. A PDMS cover was then placed on top of the gel solution, creating a channel between the gel and the PDMS for solvent flows. After 20 min, hydrogel solution polymerized and fresh medium was delivered to the channel keeping the moisture of the hydrogel. After 1 h of incubation, Fluo-4 calcium dye was loaded into the device. Following 1 more hour of incubation, sample was ready for imaging.

**ACKNOWLEDGMENTS.** We thank Prof. C. Nelson for use of the cell culture facility. Discussions with Prof. T. Gregor, Prof. J. Shaevitz, Prof. N. Wingreen, Prof. R. Austin, and Prof. S. Firestein are gratefully acknowledged. The project described was supported by Firmenich SA, Corporate R&D, Geneva, Switzerland, through a research grant.

1. Perkins TJ, Swain PS (2009) Strategies for cellular decision-making. *Mol Syst Biol* 5:326.
2. Hancock JT (2008) Cell signalling is the music of life. *Br J Biomed Sci* 65:205–8.
3. Waters C, Bassler B (2005) Quorum sensing: Cell-to-cell communication in bacteria. *Annu Rev Cell Dev Biol* 21:319–346.
4. Gregor T, Fujimoto K, Masaki N, Sawai S (2010) The onset of collective behavior in social amoebae. *Science* 328:1021–1025.
5. Barritt G (1994) *Communications Within Animal Cells* (Oxford Science Publications, Oxford, UK).
6. Tay S, et al. (2010) Single-cell NF-kB dynamics reveal digital activation and analogue information processing. *Nature* 466:267–271.
7. Smear M, Shusterman R, O'Connor R, Bozza T, Rinberg D (2011) Perception of sniff phase in mouse olfaction. *Nature* 479:397–400.
8. Lon C, et al. (1999) Defective platelet aggregation and increased resistance to thrombosis in purinergic P2Y1 receptornull mice. *J Clin Invest* 104:1731–1737.
9. Yitzhaki S, et al. (2006) Uridine-5-triphosphate (UTP) reduces infarct size and improves rat heart function after myocardial infarct. *Biochem Pharmacol* 72:949–955.
10. Burnstock G (1972) Purinergic nerves. *Pharmacol Rev* 24:509–81.
11. Burnstock G, Knight GE (2004) Cellular distribution and functions of P2 receptor subtypes in different systems. *Int Rev Cytol* 240:31–304.
12. Ferris CD, Huganir HR, Snyderc SH (1990) Calcium flux mediated by purified inositol 1,4,5-trisphosphate receptor in reconstituted lipid vesicles is allosterically regulated by adenine nucleotides. *Proc Natl Acad Sci USA* 87:2147–2151.
13. Berridge MJ (1987) Inositol trisphosphate and diacylglycerol: Two interacting second messengers. *Annu Rev Biochem* 56:159–193.
14. Berridge MJ, Irvine R (1989) Inositol trisphosphate and cell signalling. *Nature* 341:197–205.
15. Sanderson MJ, Charles AC, Boitano S, Dirksen ER (1994) Mechanisms and function of intercellular calcium signaling. *Mol Cell Endocrinol* 98:173–187.
16. Hung CT, et al. (1997) Intracellular calcium response of ACL and MCL ligament fibroblasts to fluid-induced shear stress. *Cell Signal* 9:587–594.
17. Nathanson M, et al. (1995) $Ca^{2+}$ waves are organized among hepatocytes in the intact organ. *Am J Physiol* 269:G167–71.
18. Gonzalez F, Rozengurt E, Heppel L (1989) Extracellular ATP induces the release of calcium from intracellular stores without the activation of protein kinase C in swiss 3T6 mouse fibroblasts. *Proc Natl Acad Sci USA* 86:4530–4534.
19. Mahoney MG, Slakey LL, Benham CD, Gross DJ (1998) Time course of the initial $[Ca^{2+}]_i$ response to extracellular ATP in smooth muscle depends on $[Ca^{2+}]_e$ and ATP concentration. *Biophys J* 75:2050–2058.
20. Sanderson MJ (1996) Intercellular waves of communication. *News Physiol Sci* 11:262–269.

21. Follonier L, Schaub S, Beister J, Hinz B (2008) Myofibroblast communication is controlled by intercellular mechanical coupling. *J Cell Sci* 121:3305–3316.
22. Lavado E, Snchez-Abarca LI, Tabernero A, Bolaos JP, Medina JM (1997) Oleic acid inhibits gap junction permeability and increases glucose uptake in cultured rat astrocytes. *J Neurochem* 69:721–728.
23. Dupont G, Combettes L, Bird GS, Putney JW (2011) Calcium oscillations. *Cold Spring Harb Perspect Biol* 3:a004226.
24. Chiang B, et al. (2007) Enhancing skin wound healing by direct intracellular ATP delivery. *Am J Surg* 193:213–218.
25. Monaco A, et al. (2007) Increased sensitivity to extracellular ATP of fibroblasts from patients affected by systemic sclerosis. *Ann Rheum Dis* 66:1124–1125.